Fracture Toughness of Thermally Aged Alloy 718 Weld Metal

A modified heat treatment improved the fracture toughness of Alloy 718 weldments

BY W. J. MILLS

ABSTRACT. The effects of thermal aging on fracture toughness behavior for Alloy 718 weldments were characterized using both linear elastic (K_{Ic}) and elastic-plastic (J_{Ic}) fracture mechanics techniques. Two postweld heat treatments were used in this study: a conventional heat treatment (CHT) per ASTM B637, and a modified heat treatment (MHT) that was specifically designed to improve the fracture resistance of Alloy 718 weldments. Specimens were aged at 566°C (1051°F) for up to 20,000 h and subsequently tested at 538°C (1000°F). For the MHT weld, aging resulted in a 25% reduction in J_{Ic} (100 vs. 73 kJ/m^2), and a 50% degradation in tearing modulus (13 vs. 6), with saturation occurring prior to the 5000-h exposure. Fractographic examination revealed that the reduction in fracture resistance resulted from aging-induced δ-phase precipitation which enhanced microvoid initiation.

The aged CHT weld displayed large data scatter, with some specimens failing in the elastic-plastic regime, while others exhibited a brittle fracture at K_{Ic} levels as low as 48 MPa$\sqrt{m}$. This scatter correlated with specimen-to-specimen variability in δ-precipitate morphology. Colonies of coarse δ needles, which were particularly susceptible to premature failure, formed during aging at the expense of the Laves phase. Precipitation kinetics, however, varied for each specimen, and those with high δ-phase concentrations exhibited low toughness values. The size and density of second-phase particles in both unaged and aged CHT welds were much larger than those in MHT welds, thereby accounting for the inferior CHT fracture resistance.

W. J. MILLS is with the Hanford Engineering Development Laboratory, Westinghouse Hanford Co., Richland, Wash.

Introduction

Alloy 718 is a high-strength nickel-base superalloy that exhibits good weldability and strain-age cracking resistance. Its excellent weldability properties are attributed to the sluggish precipitation kinetics of the primary strengthening γ″ (body-centered-tetragonal Ni_3Nb) phase (Refs. 1, 2), which permits relaxation of residual stresses during the initial aging treatments. For most structural applications below 650°C (1202°F), weldments are given the conventional heat treatment (CHT – Table 1) per ASTM B637 (Ref. 3). This heat treatment, however, has contributed to a series of premature failures by severely reducing the toughness of the weld fusion zone (Refs. 4–7). The poor fracture resistance resulted from the presence of Laves and δ (orthorhombic Ni_3Nb) phases in the interdendritic regions of the weld metal. To improve toughness, Idaho National Engineering Laboratory (Refs. 7, 8) developed a modified heat treatment (MHT – Table 1) that utilizes a 1093°C (1999°F) solution anneal followed by a slow cool of 55°C/h (99°F/h). The slow cooling rate reduced thermal stresses, while the high temperature anneal completely dissolved the δ phase and significantly reduced the amount of Laves phase. Compared to the CHT material, the MHT weld exhibited a seven-fold increase in J_{Ic} at 24°C (75°F) and a three-fold increase in toughness at 427° and 538°C (800° and 1000°F), without sacrificing any strength (Ref. 9). In addition to increasing the fracture resistance of weldments, the MHT improved both the fatigue crack growth (Ref. 10) and fracture toughness (Ref. 11) responses for the base metal.

Alloy 718 welds are used in structural applications in the nuclear, aerospace and petrochemical industries, where they are exposed to elevated temperatures for extended periods of time. Since this superalloy is metallurgically complex, precipitation of several metastable phases is possible and mechanical properties can be altered significantly by long-term thermal aging. The objective of this study was to monitor potential fracture toughness degradation for both CHT and MHT welds due to thermal aging. Fracture tests were performed using linear-elastic (K_{Ic})

KEY WORDS

Alloy 718 GTA Weld
Fracture Mechanics
Fracture Toughness
Linear-Elastic K_{Ic}
Elastic-Plastic J_{Ic}
Fractography
Microstructure
Heat Treatment
Precipitation Kinetics

Table 1—Precipitation Heat Treatments for Alloy 718

Conventional Heat Treatment
Annealed 1 h at 954°C (±8°C), air cooled to room temperature
Aged 8 h at 718°C (±8°C), furnace cooled to 621°C (±8°C) and held at 621°C for a total aging time of 18 h
Air cooled to room temperature
Modified Heat Treatment (Developed by Idaho National Engineering Laboratory)
Solution annealed 1 h at 1093°C (±8°C), cooled to 718°C (±8°C) at 55°C/h (±28°C/h)
Aged 4 h at 718°C, cooled to 621°C (±8°C) at 55°C/h (±28°C/h)
Aged 16 h at 621°C, air cooled to room temperature

Table 2—Chemical Composition (wt-%)

Material	C	Mn	Fe	S	Si	Cu	Ni	Cr	Al	Ti	Co	P	Mo	B	Nb	Ta
Filler metal	0.04	0.09	17.97	0.007	0.18	0.10	53.84	18.04	0.55	1.01	0.03	0.010	3.00	0.004	5.11	0.01
Base material	0.04	0.19	Bal.	0.002	0.10	<0.10	53.80	17.65	0.56	1.00	0.02	0.003	3.08	0.005	5.24	0.02

and elastic-plastic (J_{Ic}) fracture mechanics test techniques. In addition, the fracture surface micromorphology was examined to relate key microstructural features and operative fracture mechanisms to the macroscopic properties.

Experimental Procedure

Material

Weldments studied in this investigation were produced by an automatic gas tungsten arc (GTA) weld process using 1.6- × 4.1- × 28-cm (0.63- × 1.6- × 11-in.) rectangular bar stock as the base material. They had a single U-groove geometry, and were filled with 12 weld passes. Specific welding procedures are outlined in Ref. 12, and compositions for the filler metal wire and base material are given in Table 2.

The CHT and MHT test specimens were aged at 566°C for 5000, 10,000 and 20,000 h. Unaged[1] and aged microstructures are shown in Figs. 1 and 2. For the CHT weld, aging reduced the amount of Laves phase but significantly increased the size and density of the δ platelets. The relative amounts of Laves and δ phases varied significantly from specimen to specimen, especially for the 5000-h aged condition. After 10,000- and 20,000-h exposures, transformations were more complete, but considerable microstructural variability persisted. Aging of MHT welds induced precipitation of relatively fine δ needles along grain boundaries. The overall precipitate morphology was unaffected by aging time.

Figure 3 reveals that aging increased the yield and ultimate strength levels by approximately 5% for both heat-treated conditions, with saturation occurring prior to the 5000-h exposure. Saturation yield and ultimate strength levels were 960 and 1140 MPa (139 and 165 ksi), respectively, for the CHT material, and 940 and 1240 MPa (136 and 180 ksi), respectively, for the MHT material. Thermal aging reduced total elongation values for the CHT weld from 14 to 7%, whereas MHT elongation values were only reduced from 16 to 11%.

Fracture Toughness Testing

Fracture toughness tests were performed on compact specimens (Ref. 13) with the notch centered in the weld deposit and oriented parallel to the welding direction. Specimens with a width (W) of 29.3 mm (1.2 in.) and a thickness (B) of 12.7 mm (0.5 in.) were tested on an electrohydraulic closed loop machine in stroke control (stroke rate of 4.2 μm/s) at 538°C. During each test, load-line displacement values, measured by a dual LVDT technique (Ref. 14), were recorded continuously on an X-Y recorder as a function of load.

Elastic-plastic J_{Ic} concepts were used to characterize the fracture behavior for aged welds, in accordance with the multiple-specimen J_R-curve procedures outlined in ASTM Specification E813-81 (Ref. 15). An accurate measure of crack extension, Δa, for each specimen was obtained by averaging crack extension values measured at 19 positions evenly spaced across the entire crack front. The value of J was determined from the load versus load-line displacement curve by the following equation (Ref. 15):

$$J = \frac{2A\,(1+\alpha)}{Bb\,(1+\alpha^2)}$$

where: A = area under load versus load-line displacement curve, b = unbroken ligament size, and $\alpha = [(2a/b)^2 + 2(2a/b) + 2]^{1/2} - (2a/b + 1)$.

The J_R curve was constructed by plotting values of J as a function of Δa; J_{Ic} was then taken to be the value of J where a least-squares regression line through the crack extension data points intersected the stretch zone line:

$$J = 2\,\sigma_f\,(\Delta a)$$

where: σ_f = flow strength = $[\frac{1}{2}\,(\sigma_y + \sigma_u)]$, σ_y = yield strength, and σ_u = ultimate strength.

The ASTM specimen size criteria for valid J_{Ic} fracture toughness determination were met during this investigation. Values of the tearing modulus, T, were computed from the following equation (Ref. 16):

$$T = \frac{dJ}{da}\,\frac{E}{\sigma_f^2}$$

[1] *Throughout this paper, the term "unaged" refers to material that has been precipitation-hardened but not subjected to the long-term isothermal exposure.*

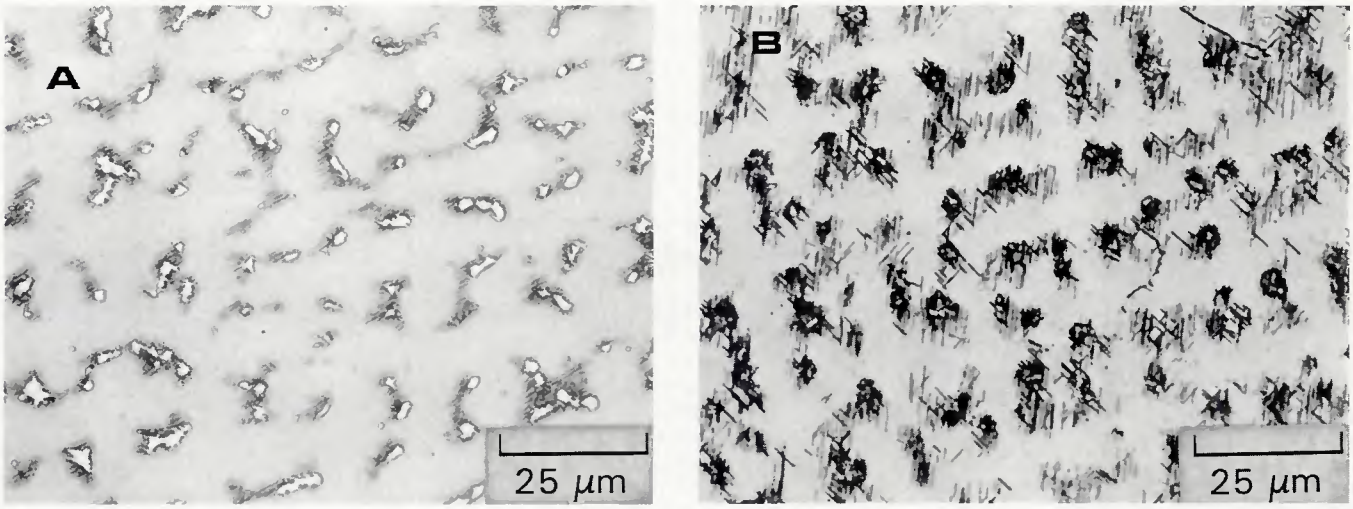

Fig. 1—Microstructure for CHT weld. A—Unaged, Laves phase surrounded by δ particles. B—Aged for 10,000 h, colonies of coarse δ precipitates that replaced the Laves phase

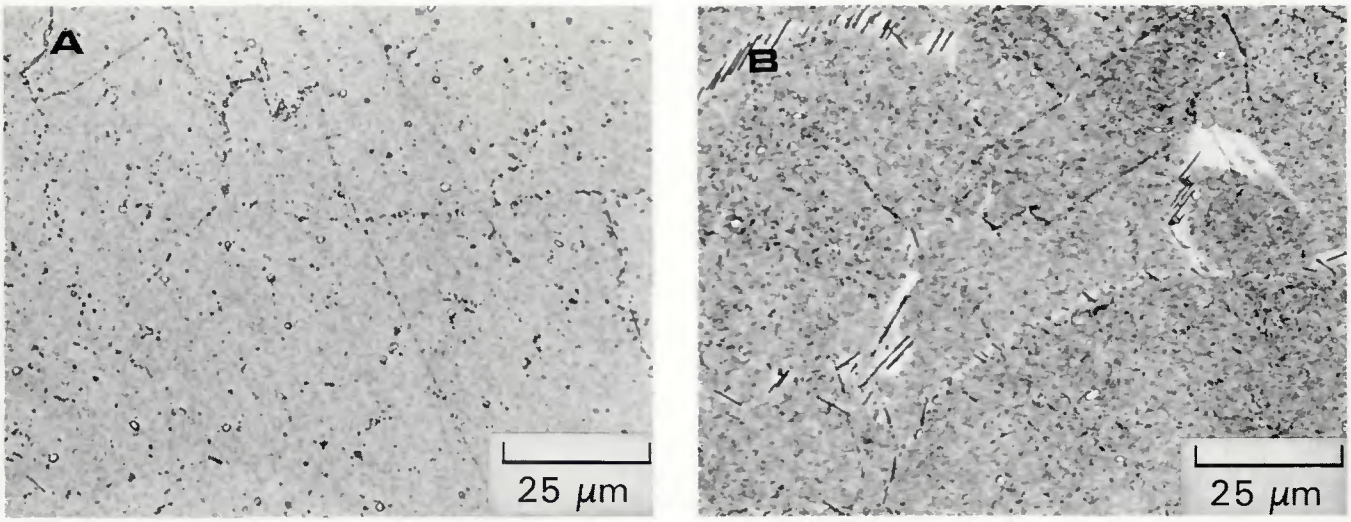

Fig. 2—Microstructure for MHT weld. A—Unaged, note Laves phase remnants (small spherical particles) distributed uniformly throughout matrix. B—Aged for 10,000 h, a few needle-like δ precipitates formed along grain boundaries

where: $dJ/da = J_R$-curve slope and E = elastic modulus.

Seven aged CHT specimens exhibited a brittle-type fracture and were therefore analyzed using linear-elastic K_{Ic} fracture mechanics procedures (Ref. 13). The ASTM test procedures and size requirements for valid K_{Ic} determinations were satisfied except for the initial precrack length. Relative crack lengths were slightly longer than the recommended a/W values of 0.45 to 0.55, but this difference is not expected to significantly affect K_{Ic} results.

Fractographic Procedures

Fractographic examination of test specimens was performed on a scanning electron microscope. To relate fracture surface appearance to key microstructural features, selected areas of fracture surfaces were electropolished so that the fracture surface topography and underlying microstructure could be studied simultaneously (Ref. 17). A protective lacquer was applied to those portions of the fracture surface that were to remain intact during electropolishing in a solution of 25-gr CrO_3, 7-ml water and 130-ml acetic acid. When electropolishing was complete, specimens were cleaned ultrasonically in acetone to remove the protective lacquer. Examination of the interfacial region between the original fracture surface and the electropolished region revealed both the fracture surface topography and underlying microstructural features.

Results and Discussion

Fracture toughness responses for the MHT weld aged to 5000, 10,000 and 20,000 h (Fig. 4) were essentially the same, demonstrating that aging effects saturate prior to the 5000-h exposure. Accordingly, all aged data were combined into a single J_R curve, yielding a J_{Ic} value of 73 ± 4 kJ/m² and a tearing modulus of 6. Saturation J_{Ic} and T levels for the aged weld were approximately 25 and 50% lower than their unaged counterparts. Equivalent plane strain fracture toughness K_{Jc} values of 136 and 116 MPa $\sqrt{m}$ for the unaged and aged welds, respectively, were computed from experimental J_{Ic} values by the following equation (Ref. 18):

$$K_{Jc} = \sqrt{\frac{J_{Ic} E}{1 - \nu^2}}$$

where ν represents Poisson's ratio.

The modest reduction in K_{Ic} after exposures up to 20,000 h indicates that the MHT weld retains good fracture resistance. At toughness levels above 116 MPa $\sqrt{m}$, thicknesses greater than 40 mm (1.6 in.) are required to produce sufficient constraint for a plane strain fracture. Therefore, for most structural MHT Alloy 718 weldments, where thicknesses are generally limited to approximately 10 mm (0.4 in.), brittle plane strain fracture conditions cannot develop.

The reduction in MHT fracture toughness resulted from formation of needle-like δ precipitates during aging. In the unaged conditions, crack growth occurred by a microvoid coalescence mechanism initiated by Laves-phase remnants, as illustrated in Fig. 5A. After aging, however, both Laves and δ phases served as microvoid nucleation sites (Fig. 5B), accounting for the reduction in J_{Ic}

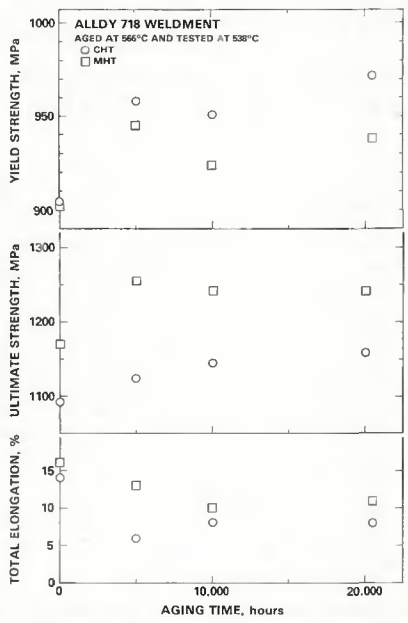

Fig. 3—Effect of long-term thermal aging on tensile properties

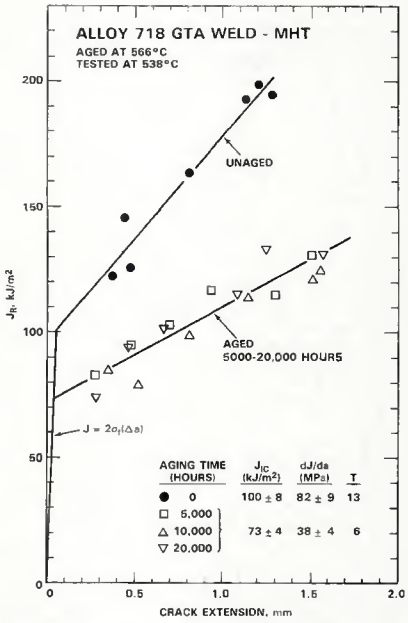

Fig. 4—J_R curves for unaged and aged MHT weld

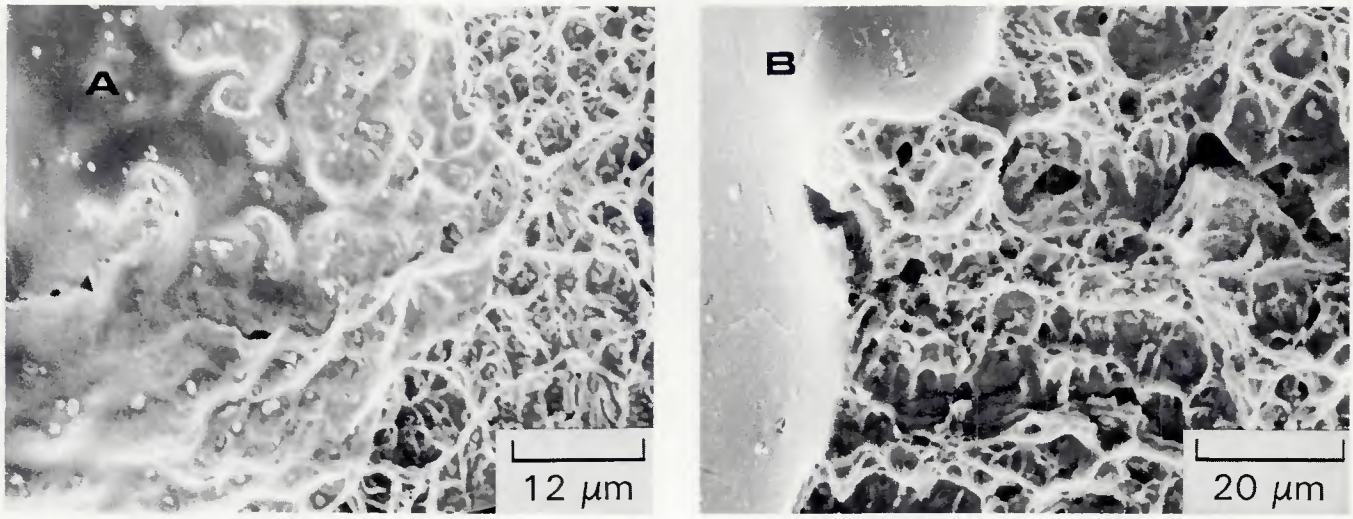

Fig. 5—Metallographic-fractographic profile for MHT welds. A—Unaged, dimples initiated exclusively by decohesion of the Laves phase remnants from the matrix. B—Aged, microvoids nucleated by both Laves and δ phases

and T. Indeed, the fracture toughness response for the aged MHT weld agreed with that observed in CHT base metal (J_{Ic} = 59–83 kJ/m^2, T = 8–11), where microvoid nucleation at δ platelets controlled the fracture process (Ref. 11).

The J_R curve for unaged CHT weld and individual J versus Δa data points for the aged material are represented in Fig. 6. While the unaged CHT weld exhibited slightly more relative scatter than its MHT counterpart, the aged weld displayed extensive scatter, which precluded construction of meaningful J_R curves. After aging to 5000 h, half of the specimens showed a definite improvement in fracture resistance, whereas the other half demonstrated a degradation in toughness, relative to the unaged material. The variability in fracture toughness response was readily apparent in the load-displacement curves. After longer exposures, approximately half of the specimens showed little or no net change in toughness, while the remaining ones exhibited a brittle, plane strain fracture response, with ASTM valid K_{Ic} values ranging from 48 to 64 MPa$\sqrt{m}$. The K_{Ic} fracture toughness results are summarized in Table 3. Values of K_{Ic} were not reported for high toughness specimens because they did not meet ASTM E399 plasticity ($P_{max}/P_Q < 1.10$) or plane strain [B,a,W-a > 2.5 $(K_{Ic}/\sigma_{ys})^2$] criteria. Since the highly embrittled specimens failed by a rapid, stable tearing process, tests were interrupted prior to final separation so that J and Δa values could also be determined. These results are plotted in Fig. 6.

The large scatter for the CHT welds was due to microstructural variability. In the unaged material, tearing occurred by a microvoid coalescence process initiated by Laves and δ precipitates, with the larger particles being particularly prone to premature failure. During aging, the blocky Laves particles were partially dissolved, whereas the size and density of the δ platelets were increased. Nucleation and growth rates for the δ phase, however, varied significantly from specimen to specimen, as shown in Fig. 7. Those specimens with high δ phase concentrations exhibited low toughness values.

Direct comparison of fracture surface morphologies for high and low toughness specimens aged for 5000 and 10,000 h is made in Figs. 8 and 9. These four fractographs correspond to the four data points denoted by asterisks on Fig. 6. For the high toughness specimen exposed for 5000 h, the aging time was sufficient to reduce the size of the Laves particles, but

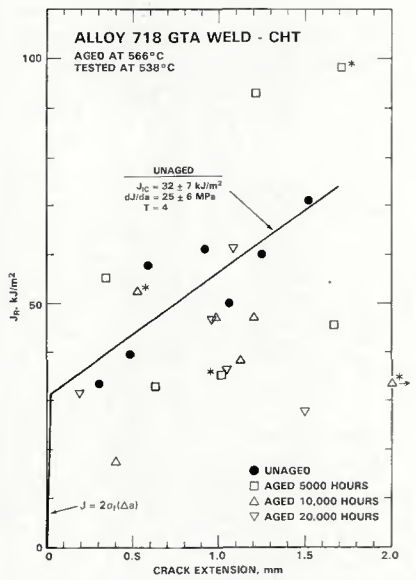

Fig. 6—Summary of fracture toughness response for unaged and aged CHT welds. Asterisks refer to specimens whose fracture surfaces are illustrated in Figs. 8, 9

Table 3—Summary of K_{Ic} and K_Q Fracture Toughness Results for Aged CHT Welds

Specimen Number	Aging Time (h)	Thickness (mm)	Width (mm)	Crack Length (mm)	P_Q kN	K_Q[a] MPa$\sqrt{m}$	$\frac{P_{max}}{P_{min}}$	$2.5\left(\frac{K_Q}{\sigma_{ys}}\right)^2$ (mm)	K_{Ic} MPa$\sqrt{m}$
2130	5000	12.59	29.28	16.96	13.8	81	1.17	17.6	–
2133	5000	12.57	29.26	19.00	7.5	58	1.09	9.1	58
2135	5000	12.62	29.28	18.96	10.5	81	1.17	17.6	–
2137	5000	12.63	29.31	19.16	9.7	77	1.13	15.8	–
2142	5000	12.62	29.28	19.05	8.1	64	1.08	10.8	–
2126	10,000	12.59	29.30	18.79	8.3	63	1.17	10.6	–
2128	10,000	12.60	29.31	19.15	6.4	50	1.06	7.8	50
2132	10,000	12.61	29.30	18.93	6.2	48	1.07	6.2	48
2136	10,000	12.62	29.29	18.65	10.2	75	1.09	15.2	–
2144	10,000	12.60	29.26	18.83	8.1	62	1.09	10.2	62
2149	10,000	12.61	29.29	19.10	7.8	61	1.17	10.1	–
2127	20,000	12.55	29.28	19.44	7.4	62	1.09	10.1	–
2131	20,000	12.60	29.29	19.70	5.7	50	1.05	6.6	50
2138	20,000	12.60	29.32	16.64	13.2	74	1.12	14.7	–
2139	20,000	12.59	29.30	16.41	11.6	63	1.04	10.7	63

[a]Critical load (P_Q) values determined by the 5% secant offset method were used to determine K_Q, in accordance with ASTM E399-81. K_Q was equal to K_{Ic} when the ASTM plasticity and plane strain size requirements (Sections 9.1.2 and 9.1.3 of ASTM E399-81) were met.

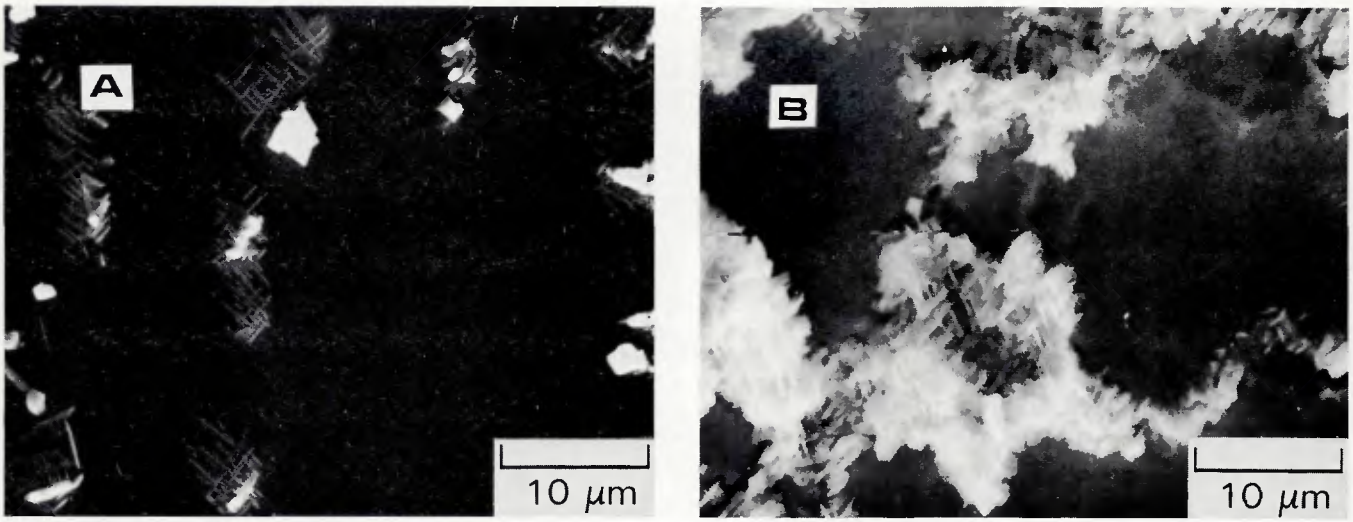

Fig. 7—Electropolished metallographic profiles for two CHT welds aged for 10,000 h. Note the variability in second phase morphology. A—In high toughness specimens, the blocky Laves phase was partially dissolved, but there was no significant increase in the density of δ precipitates. B—In specimens exhibiting inferior fracture resistance, colonies of coarse δ needles replaced the Laves phase

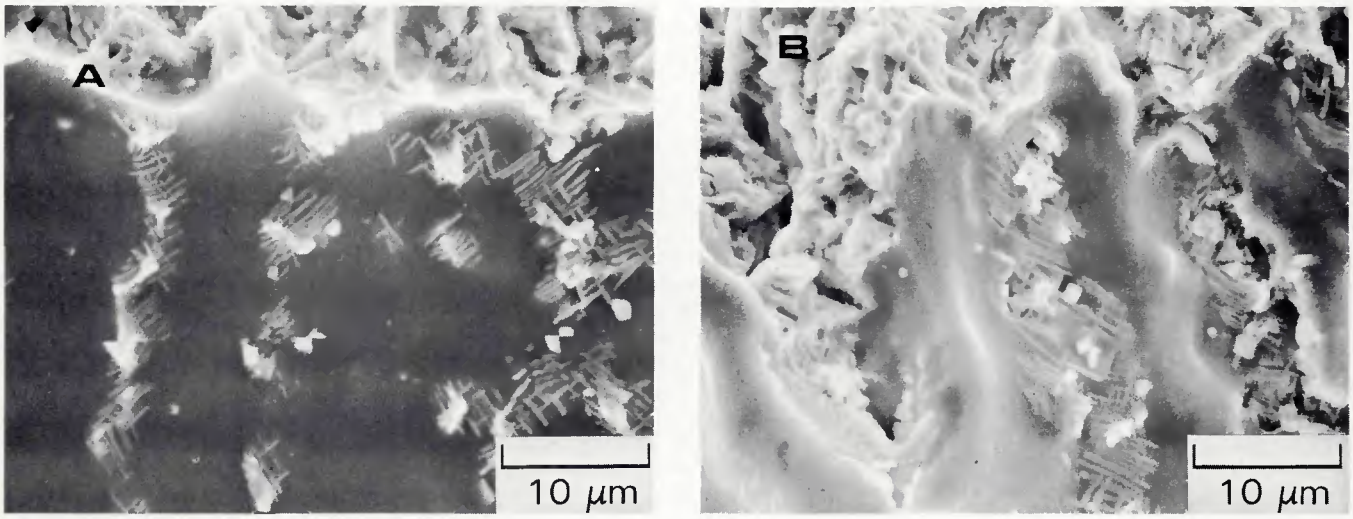

Fig. 8—Metallographic-fractographic interface for 5000-h aged CHT specimens, illustrating typical dimple rupture mechanism. A—High toughness specimen, where aging partially dissolved the Laves particles, making them more fracture resistant. The δ platelet morphology was essentially unaltered by aging. B—Low toughness specimen. Note the significantly higher density of δ needles, which provided additional microvoid nucleation sites

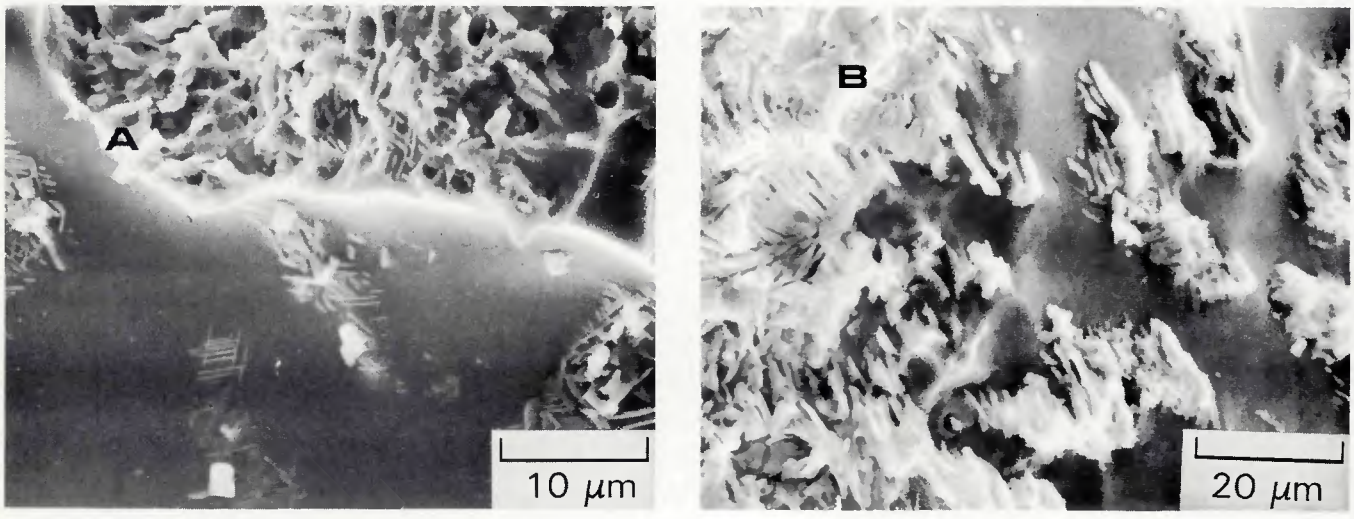

Fig. 9—Metallographic-fractographic profile for CHT specimens aged for 10,000 h, showing microvoid initiation sites. A—In intermediate toughness specimens, Laves particles were partially dissolved and the density of δ platelets remained relatively low. B—Low toughness specimens exhibited colonies of coarse δ platelets. Entire colonies served as microvoid nucleation sites, as shown on the left side of this fractograph

it was not long enough to increase the δ platelet density. Hence, its fracture resistance was superior to that for the unaged material. For its low toughness counterpart, the 5000-h exposure induced significant δ-phase precipitation, thereby degrading the fracture toughness relative to the unaged weld.

Similarly, the extent of δ phase precipitation dictated the fracture toughness response for CHT welds after 10,000- and 20,000-h agings. At the longer exposures, some specimens exhibited only a modest increase in δ platelet density. This caused a slight degradation in fracture resistance, which was offset by the partial dissolution of Laves particles. The net result was essentially no change in toughness relative to the unaged material. By contrast, low toughness specimens exhibited large δ platelet colonies (Fig. 7B) that were susceptible to premature failure. Figure 9B reveals that an entire δ colony often initiated a single, large microvoid. Subsequent coalescence of these large voids caused a premature advance of the crack and resulted in an overall brittle fracture mode.

Most welded components contain crack-like flaws because it is not practical to fabricate completely defect-free structures. Through effective quality control and NDE inspection, defect size can be minimized, but complete elimination is unrealistic. Classical design analyses provide protection against premature failure of defect-free components, but do not generally address the integrity of flawed structures. To verify protection against brittle fractures, a fracture mechanics assessment is required, based on the supposition of a readily detectable flaw in the most severely challenged location and orientation.

The overall flaw sensitivity for CHT Alloy 718 weldments can be addressed by establishing a unique relationship between fracture toughness, design allowable stress limit and critical flaw size. First, it is important to account for variability in the weld's fracture behavior to determine minimum-expected toughness values for use in design and safety analyses. In this study, a lower-bound approach was adopted to establish the minimum-expected K_{Ic} value (48 MPa $\sqrt{m}$ for the 10,000- to 20,000-h aged CHT weld) because the excessive data scatter precluded a meaningful statistical analysis. For the unaged CHT weld, the fracture toughness was assumed to be 76 MPa $\sqrt{m}$ (Ref. 9), which corresponds to the equivalent K_{Ic} value determined from the experimental J_{Ic} value of 32 kJ/m^2.

For CHT Alloy 718 components at 538°C (1000°F), the ASME Code (Ref. 19) maximum allowable stress limit is approximately 365 MPa (53 ksi), which corresponds to one-third of the ultimate tensile strength. By assuming a maximum design stress of 365 MPa for a 10-mm (0.4-in.) thick weldment containing a surface crack with an a/c ratio of 0.33 (in keeping with the general approach of Appendix G, Section III, of the ASME Code—Ref. 19), critical flaw sizes were found to range from 7 mm (0.3 in.) for the unaged weld to 4 mm (0.2 in.) after 10,000 and 20,000 h exposures at 566°C (1051°F). These relatively small critical flaw sizes demonstrate that fracture mechanics analysis, coupled with effective NDE procedures, should be an integral part of structural integrity evaluations for welded CHT components.

The superior fracture resistance of the MHT weld results in substantially larger critical flaw sizes. Indeed, for a design stress of 365 MPa, through-thickness crack lengths (2c) in excess of 60 mm (2.4 in.) would be required to initiate fracture. Brittle fracture is, therefore, not a primary concern for welded MHT components; however, fracture control based on fracture mechanics concepts should still be considered for critical engineering components to provide a safety margin beyond classical design.

Conclusions

The effects of thermal aging on the fracture toughness of conventional and modified heat-treated Alloy 718 weldments were characterized using both linear-elastic K_{Ic} and elastic-plastic J_{Ic} fracture mechanics concepts. The results are summarized below:

1. Aging at 566°C reduced the J_{Ic} and tearing modulus for the MHT weld by approximately 25 and 50%, respectively. Toughness degradation was found to saturate prior to the 5000-h exposure. For a stress limit design approach where the applied stress (365 MPa) is one-third the ultimate strength, critical flaw sizes are on the order of 60 mm, demonstrating that MHT welds retain good fracture resistance after aging.

2. The reduction in fracture toughness for the MHT weld resulted from aging-induced δ precipitates, which served as microvoid nucleation sites.

3. Aging of the CHT weld greatly increased specimen-to-specimen variability in fracture toughness behavior. Under comparable aging conditions, some specimens failed under elastic-plastic conditions, whereas others exhibited a brittle, plane strain fracture response, with K_{Ic} levels as low as 48 MPa $\sqrt{m}$.

4. This large data scatter was directly correlated with microstructural variations. The high temperature exposure partially dissolved the blocky Laves particles from the weld zone, and in their place a network of coarse, needle-like δ particles formed. The size and density of the δ precipitates, however, varied significantly from specimen to specimen, and those with high δ phase concentrations were found to exhibit inferior toughnesses.

5. The present results demonstrate that aged CHT welds are susceptible to brittle fracture. For example, at an ASME Code allowable maximum stress level of 365 MPa, critical flaw sizes are on the order of 4 mm. Therefore, total structural integrity assessments for welded construction of CHT Alloy 718 components necessitates the combined use of classical design and fracture mechanics analyses.

Acknowledgments

This paper is based on work performed under U.S. Department of Energy Contract DE-AC06-76FF02170, with Westinghouse Hanford Company, a subsidiary of Westinghouse Electric Corporation. The author wishes to gratefully acknowledge W. D. Themar for performing the fracture toughness tests and B. Mastel for performing the electron microscopy.

References

1. Prager, M., and Shira, C. S. 1968. Welding of precipitation-hardening nickel-base alloys. Welding Research Council, Bulletin No. 128.

2. Duvall, D. S., and Owczarski, W. A. 1969. Studies of postweld heat-treatment cracking in nickel-base alloys. *Welding Journal* 48(1):10-s to 22-s.

3. Precipitation hardening nickel alloy bars, forgings and forging stock for high-temperature service. 1984. ASTM Specification B637-84, *1984 Annual Book of ASTM Standards,* Vol. 02.04, pp. 724-730, American Society for Testing and Materials, Philadelphia, Pa.

4. Gordine, J. 1971. Some problems in welding Inconel 718. *Welding Journal* 50(11):480-s to 484-s.

5. Graber, M. J., Brinkman, C. R., and Hobbins, R. R. 1975. Metallurgical evaluation of welding and heat treating procedures for the Inconel 718 PBF in-pile tube. Report ANCR-1087, Aerojet Nuclear Company, Idaho Falls, Idaho.

6. Smolik, G. R. 1974. Analyses of failure which occurred during heat treatments in the Inconel 718 PBF acoustic filter. Report ANCR-1178, Aerojet Nuclear Company, Idaho Falls, Idaho.

7. Smolik, G. R., and Reuter, W. G. 1975. Heat treatment versus properties studies associated with the Inconel 718 PBF acoustic filters. Technical Report No. 493, Aerojet Nuclear Company, Idaho Falls, Idaho.

8. Reuter, W. G. 1977. Design data for the ¼-in. thick Alloy 718 in-pile tube. Report TREE-NUREG-1087, EG&G Idaho, Inc., Idaho Falls, Idaho.

9. Mills, W. J. 1984. Effect of heat treatment on the tensile and fracture toughness behavior of Alloy 718 weldments. *Welding Journal* 63(8):237-s to 245-s.

10. Mills, W. J., and James, L. A. 1978. Effect of heat-treatment on elevated temperature fatigue-crack growth behavior of two heats of

Alloy 718. ASME Publication 78-WA/PVP-3.

11. Mills, W. J. 1980. The effect of heat treatment on the room temperature and elevated temperature fracture toughness response of Alloy 718. *Journal of Engineering Materials and Technology* 102:118-126.

12. Mills, W. J. 1979. The influence of heat-treatment on the microstructure and mechanical properties of Alloy 718 base metal and weldments. Report HEDL-TME 78-54, Westinghouse Hanford Company.

13. Plane strain fracture toughness of metallic materials. 1983. ASTM Specification E399-81, *1982 Annual Book of ASTM Standards,* Part 10, pp. 592-622, American Society for Testing and Materials, Philadelphia, Pa.

14. Mills, W. J., James, L. A., and Williams, J. A. 1977. A technique for measuring load-line displacements of compact ductile fracture toughness specimens at elevated temperatures. *Journal of Testing and Evaluation* 5(6):446-451.

15. J_{Ic} a measure of fracture toughness. 1982. ASTM Specification E813-81, *1982 Annual Book of ASTM Standards,* Part 10, pp. 822-840, American Society for Testing and Materials, Philadelphia, Pa.

16. Paris, P. C., Tada, H., Zahoor, A., and Ernst, H. 1979. The theory of instability of the tearing mode for elastic-plastic crack growth. *Elastic-Plastic Fracture,* ASTM STP 668, pp. 5-36, American Society for Testing and Materials, Philadelphia, Pa.

17. Chesnutt, J. C., and Spurling, R. A. 1977. Fracture topography microstructure correlations in SEM. *Metallurgical Transactions,* Vol. 8A, pp. 216-218.

18. Begley, J. A., and Landes, J. D. 1974. The J-integral as a fracture criterion. *Fracture Toughness,* ASTM STP 514, pp. 1-20. American Society for Testing and Materials, Philadelphia, Pa.

19. ASME Boiler and Pressure Vessel Code, American Society of Mechanical Engineers, 1980.